FULL PAPER

Compartmentalized Thin Films

ADVANCED
FUNCTIONAL
MATERIALS
www.afm-journal.de

Compartmentalized Thin Films with Customized Functionality via Interfacial Cross-linking of Protein Cages

Aijie Liu, Mark V. de Ruiter, Wei Zhu, Stan J. Maassen, Liulin Yang,* and Jeroen J. L. M. Cornelissen*

Hybrid thin films with a high loading and homogeneous dispersion of functional nanoparticles (and/or molecules) find applications in (bio)-sensors and electronic devices. The fabrication of such hybrid thin films, however, suffers from the complex and diverse surface and physicochemical properties of individual nanoparticles. To address this challenge, a facile and general strategy toward compartmentalized thin films through the interfacial cross-linking of viral protein cages is reported. Employing these protein cages, gold nanoparticles, as well as enzyme horseradish peroxidase, are encapsulated into virus-like particles and then cross-linked into thin films with a thickness varying from monolayer to submicron dimensions. These compartmentalized thin films not only ensure that the cargo is homogeneously dispersed, but also display good catalytic activity. This strategy is, in principle, applicable for a wide range of (bio)-organic nanocontainers, enabling the versatile fabrication of 2D thin films with extensive application prospects.

1. Introduction

Hybrid thin films with integrated nanoparticles (NPs) find intriguing applications in material science and nanodevices, for e.g. selective separation,[1,2] catalysis,[3] and sensors.[4,5] This integration of functional NPs, large molecules, or bioactive enzymes into thin films offers numerous advantages to tailor the structural and functional properties by well-defined design. To this date, several strategies have been developed to prepare such hybrid thin films including surfactant templating,[6] spinning-assisted assembly,[7] layer-by-layer deposition, and cross-linking.[8–11] These strategies that deal directly with NPs

or macromolecules, often suffer from the complex and diverse surface and physico-chemical properties of the individual NPs or the substantial loss of enzyme activity during crosslinking.[8] To address this challenge, a generally applicable strategy, which involves integrating nanocarriers together with their cargo into compartmentalized thin films, is proposed in this work. Ferritin and viral particles such as the Cowpea Mosaic Virus, Tobacco Mosaic Virus, P22, and Turnip Yellow Mosaic Virus, are able to assemble into ordered 2D or 3D arrays at interfaces.[12–20] Inspired by this well-defined assembly, the interfacial cross-linking of uniform and adaptable nanocarriers, e.g., protein cages, into thin films with the capacity to encapsulate various "cargos" without affecting their surface properties or activities, is suggested. This will allow a broad spectrum of functional building blocks to be organized into hierarchical architectures relevant to applications such as energy transduction, sensing, catalysis, and smart membranes.[9,15]

Viral protein cages, derived from viruses such as the Cowpea Chlorotic Mosaic Virus (CCMV), are natural biomaterials with uniform size and shape that are formed by the controlled self-assembly of coat proteins, and can be functionalized in a robust and well-defined manner.[21–26] By taking advantage of the reversible assembly/disassembly properties of the CCMV protein cages, the inner space can be loaded with inorganic NPs, enzymes, polymers, and organic aggregates resulting in functional virus-like particles (VLPs).[27–30] Combining the encapsulation abilities of VLPs with their diverse surface chemistry, we explored the strategy to prepare viral protein cage-based (free-standing) thin films with customized functionality via interfacial crosslinking of the constituent proteins. The abundant number of amine groups on the exterior surface of protein cages allows the interfacial cross-linking.[31,32] Through careful control of the reactant concentration and reaction time, films can be formed on a water/oil interface and the thickness is tunable from a monolayer to submicron size. Moreover, based on the versatile loading ability of CCMV protein cages, gold NPs and the enzyme horseradish peroxidase (HRP) have been efficiently integrated into these thin films as model systems (**Scheme 1**). The resultant gold NP hybrid thin film and enzymatic HRP thin film display catalytic activity as expected, showing the straightforward introduction of functionality into the hybrid thin films.

Dr. A. Liu, M. V. de Ruiter, S. J. Maassen, Dr. L. Yang, Prof. J. J. L. M. Cornelissen
Laboratory for Biomolecular Nanotechnology
MESA+ Institute for Nanotechnology
University of Twente
PO Box 217, 7500 AE Enschede, The Netherlands
E-mail: l.yang-2@utwente.nl; j.j.l.m.cornelissen@utwente.nl
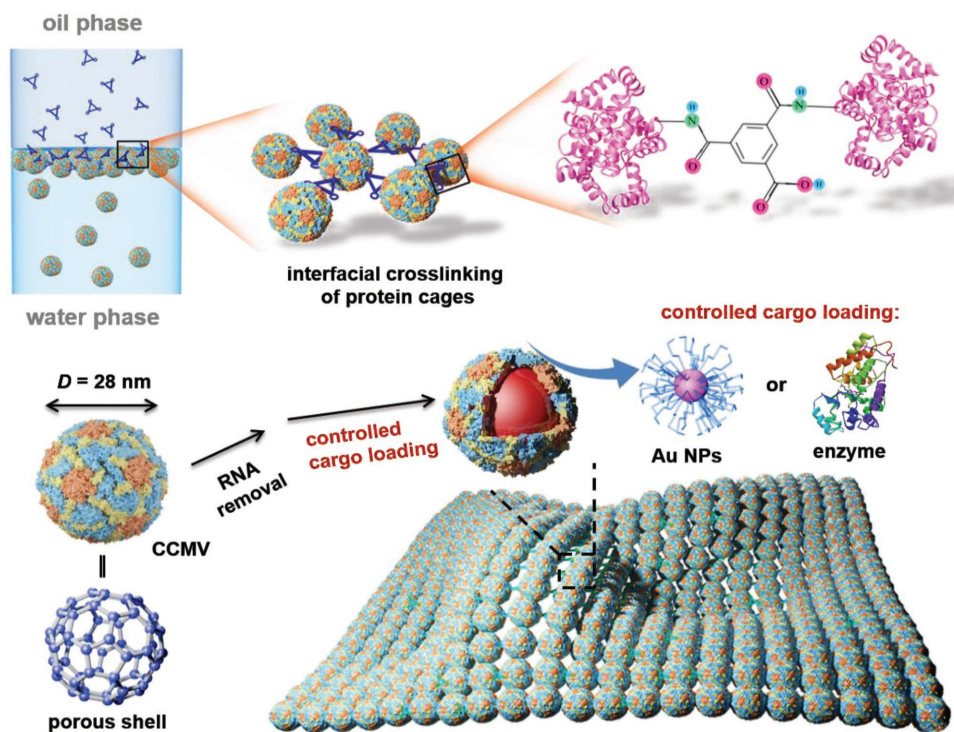Dr. W. Zhu[+]
Molecular Nanofabrication Group
University of Twente
PO Box 217, 7500 AE Enschede, The Netherlands

**ADVANCED
SCIENCE NEWS**
www.advancedsciencenews.com

**ADVANCED
FUNCTIONAL
MATERIALS**
www.afm-journal.de

Scheme 1. Schematic representation of the fabrication of compartmentalized thin films with customized functionality by interfacial crosslinking.

2. Results and Discussion

2.1 Interfacial-Crosslinking of CCMV into Thin Films

Thin films based on CCMV protein cages were prepared by interfacial crosslinking at the oil–water interface using trimesoyl chloride (TMC) as a cross linker (Scheme 1). CCMV protein cages with particle size of $D = 28$ nm (**Figure 1**a) were isolated from infected plants according to a reported method,[1] and redispersed in a phosphate-buffered saline solution (PBS, pH 7.2) as the bottom layer. Subsequently, TMC as a cross-linker dissolved in hexane phase was gently added as the top layer. Based on the diffusion and migration of both CCMV NPs and TMC molecules towards the interfacial surface, a (free-standing) thin film formed at the interface through amidation reactions between carboxyl chlorides from TMC and amine groups from CCMV. To demonstrate the customized functionalization of this hybrid thin film system, an Au NPs integrated thin film and an enzyme HRP integrated ultrathin film have been fabricated following the same protocol using Au NPs or HRP loaded VLPs, respectively.

The thin film formed at the water/oil interface was visible by naked eye and its presence was further confirmed by a water droplet test. When a droplet of aqueous Black T solution was dropped into the biphasic solution, the small droplet finally stayed at the interface (Figure 1b), indicating the presence of a thin film. Moreover, the thin film can tolerate a certain extent of deformation without rupture when the droplet on top of the film is poked lightly (Figure S1a, Supporting Information). In a control experiment, the droplet would directly pass through the interface into aqueous phase when there is no thin film at the

interface (Figure S1b, Supporting Information). Furthermore, when transferred to a copper electron microscopy grid, a transparent, free-standing thin film was observed by optical microscopy (Figure 1c). All this information confirmed the successful fabrication of CCMV protein cage-based free-standing thin film.

Infrared (IR) spectroscopy studies show that, as expected, the TMC concentration and reaction time influence the degree of CCMV crosslinking. The obtained films were transferred to polyacrylonitrile ultrafiltration membranes (PAN, SolSep, Netherlands) for characterization. The C≡N stretching mode ($v = 2242$ cm^{-1}) from PAN was used as an internal reference, while the degree of crosslinking of the film was monitored by the increasing signal originating from the amide group (N−H$_{bend}$ $v = 1650$ cm^{-1}, C=O$_{stretch}$ $v = 1540$ cm^{-1}) (Figure 1d).[3] The amide absorption bands initially increased with increasing TMC concentration, while beyond 0.25 wt% the intensity leveled off (Figure 1d,e). The cross-linking between virus particles and TMC faces competition with the hydrolysis of TMC, which decreases the available cross-linkers and furthermore acidifies the aqueous solution. The latter reduces the reactivity of the basic, amine groups present on the virus shell by protonation. At a low concentration of TMC (<0.125 wt%), the amount of TMC at the interface is insufficient to crosslink the virus particles, while at higher concentrations (>0.25 wt%), the excess TMC molecules at the interface passivate most of the reactive amine groups on the virus shell and prevent them from cross-linking.

The degree of cross linking, and presumably the film thickness, also depends on the reaction time. As shown in Figure 1e bottom image (IR spectrum shown in Figure S2, Supporting Information), the IR intensity of the amide group increases within the first 15 min of the reaction. After 15 min, the
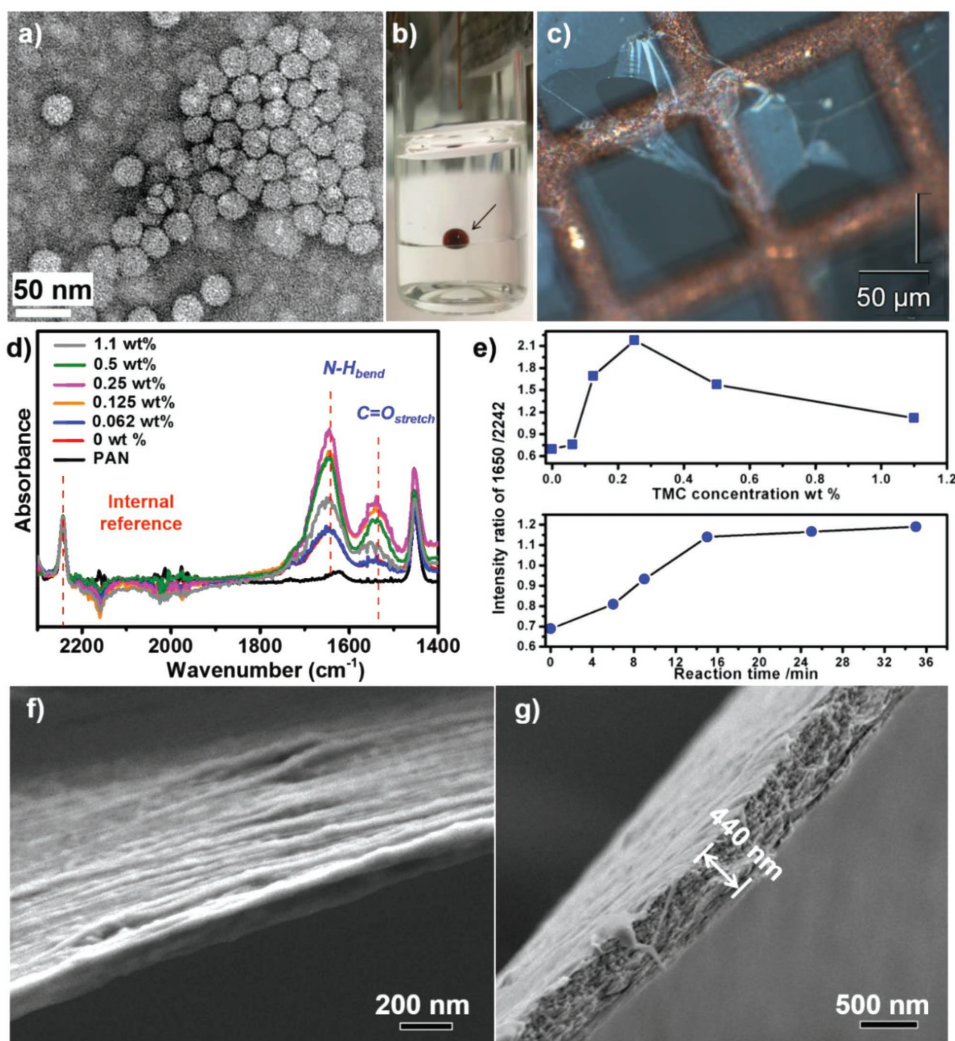
**ADVANCED
SCIENCE NEWS**

www.advancedsciencenews.com

**ADVANCED
FUNCTIONAL
MATERIALS**

www.afm-journal.de

Figure 1. a) TEM image of CCMV nanoparticles stained by 1 wt% uranyl acetate; Optical image of the CCMV protein cage based free-standing thin film with an aqueous drop on b) top or on c) a copper gird; d) FTIR spectra of CCMV powder, PAN support, and PAN supported free-standing thin films prepared with varied TMC concentrations; e) Plots of intensity ratio of signals at the $k = 1650$ cm^{-1} (N−H bending, amide group) to $k = 2242$ cm^{-1} (C≡N stretching in PAN) versus TMC concentration (e, top) and reaction time (e, bottom). SEM images of thin films formed with 1.5 mg mL^{-1} of CCMV and 0.25 wt% TMC at different reaction time f) 15 min and g) 14 h.

increase of IR signal levels off, indicating a decreasing growth and/or cross-linking of the film. After the initial 15 min of reaction, the thickness of the film as measured by scanning electron miscroscopy (SEM) is in line with the dimension of a few virus nanoparticles (Figure 1f). After 14 h, the thickness of the film reached 440 nm, containing about 15 layers of CCMV NPs (Figure 1g). The slower film growth after 15 min is likely due to a barrier effect of the formed monolayer film that hampers the diffusion of TMC molecules and virus particles across this film and in that way, inhibits the cross-linking.

2.2. Compartmentalized Thin Films with Customized Functionality

The films obtained in this way can be equipped with different properties by crosslinking VLPs with functional cargo. This allows for the straightforward quantification of the loading inside the film and increased stability of this cargo. Furthermore, since the surface property of the protein cage remains the same with varying cargo, the chemistry established in this section can be applied to construct films with different functionalities. Two representative examples are given to show the versatility of this strategy.

2.3. Compartmentalized Thin Films with Gold Nanoparticles Loaded

For the first example, CCMV-based VLPs containing 7 nm, bis(p-sulfonatophenyl)phenylphosphine stabilized gold NPs (Au7B) (denoted as CCMV-Au7B) were prepared following procedures previously reported by van us.[27] The obtained hybrid VLPs (CCMV-Au7B) formed a thin film analogous to the
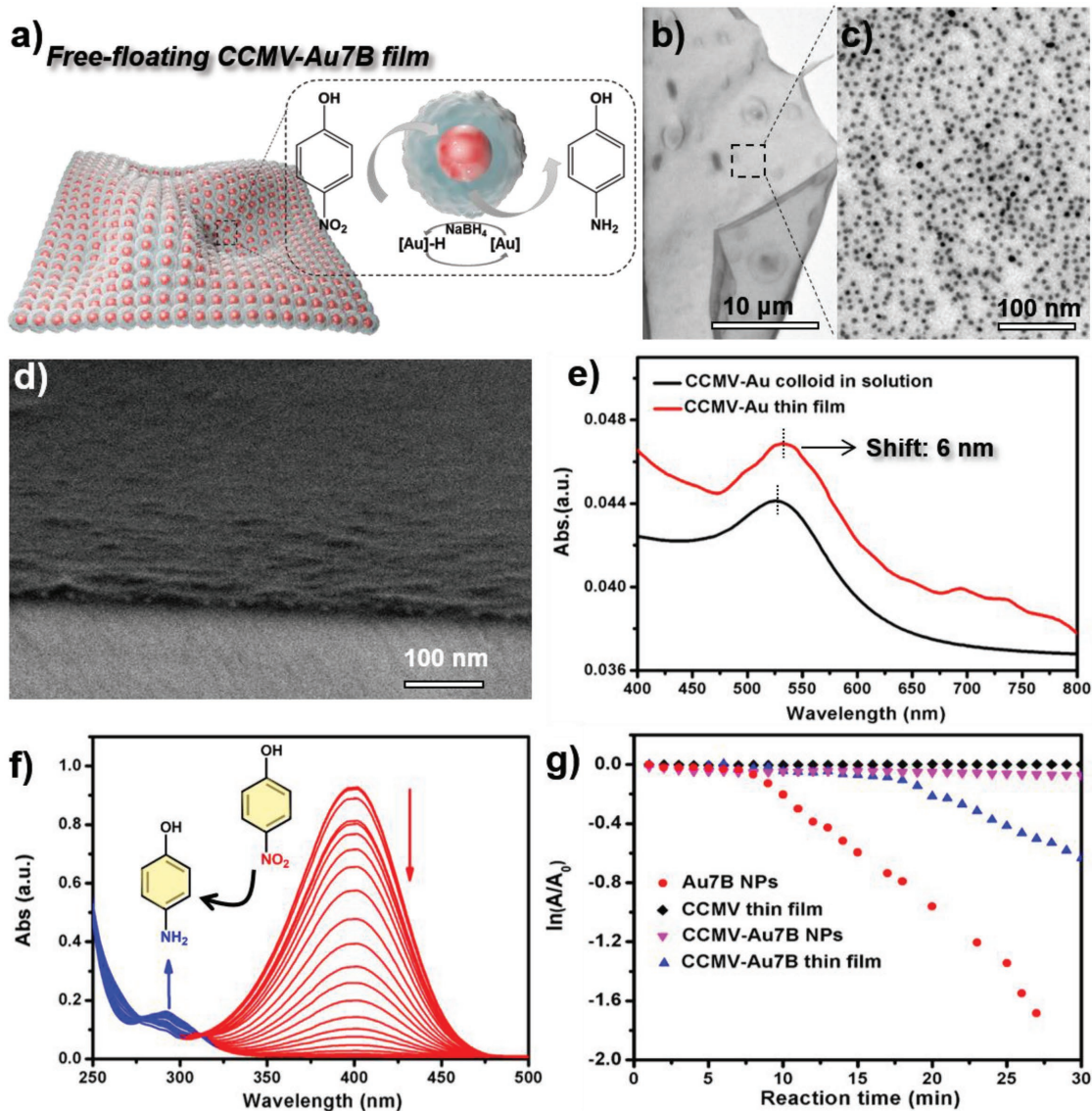
**ADVANCED
SCIENCE NEWS**
www.advancedsciencenews.com

**ADVANCED
FUNCTIONAL
MATERIALS**
www.afm-journal.de

Figure 2. a) Schematic illustration of the fabrication of a CCMV-Au7B based free-standing film; TEM images of CCMV-Au7B films with b) low magnification and c) high magnification; d) SEM analysis of CCMV-Au7B monolayer; e) UV–vis spectra of CCMV-Au7B VLPs in buffer solution and in the film formed after 15 min; f) Reduction of 4-nitrophenol monitored by UV–vis spectroscopy; g) Kinetic analysis of the catalytic reductions carried out by Au NPs, CCMV-Au7B VLPs, a CCMV thin film and the CCMV-Au7B thin film.

CCMV NPs, and its catalytic activity was studied (**Figure 2**a). The formed CCMV-Au7B films were characterized by transmission electron microscopy (TEM), SEM, atomic force microscopy (AFM), and UV–vis spectroscopy. TEM with a low magnification showed, a folded film on top of the grid (Figure 2b). Upon zooming, the Au NPs are found to be dispersed and densely packed but without aggregation across the whole film (Figure 2c). A single layer of NPs was clearly observed on the film edge by SEM (Figure 2d) and AFM (Figure S3, Supporting Information). Compared to dissolved CCMV-Au7B NPs, the formed CCMV-Au7B film has a slightly red-shifted (≈6 nm) absorption at $\lambda = 532$ nm in the UV–vis spectrum (Figure 2e), suggesting that a substantial part of the gold nanoparticles is densely packed in the film. In a control experiment, the red-shift was not observed for a film prepared from VLPs con-

taining tannic acid stabilized gold nanoparticles (Figure S4a, Supporting Information). In that case, the empty VLPs present in these samples dilute the gold nanoparticles in the film and consequently increase the gold–gold distance diminishing the local surface-plasmon resonance (LSPR) effect.[33–35] All of the results verify that the compartments in the film that originate from the protein cages can effectively separate and stabilize gold nanoparticles at high concentrations without aggregation.

To explore the catalytic activity of the formed CCMV-Au7B monolayer film, the reduction of 4-nitrophenol (4-NP) to 4-amini-phenol, as a model reaction, was monitored by UV–vis spectroscopy (Figure 2f). As the reaction proceeds, the absorption of 4-NP at $\lambda = 400$ nm decreases, accompanied by an increase of the absorption at $\lambda = 292$ nm, in line with the generation of the product 4-aminophenol. In control experiments, the reduction of

**ADVANCED
SCIENCE NEWS**
www.advancedsciencenews.com

**ADVANCED
FUNCTIONAL
MATERIALS**
www.afm-journal.de

4-NP catalyzed by CCMV-Au7B VLPs and a CCMV film was also carried out under the same conditions. Reaction rates were calculated from plotting $\ln(A/A_0)$ versus the reaction time, in which A_0 is the initial absorption intensity at $\lambda = 400$ nm, and A is the real-time absorption intensity at the same wavelength (see for details of the calculation, Section S1.2.2, Figures S5 and S6,Supporting Information). For the CCMV film without Au NPs, as expected, no catalytic activity was observed (Figure 2g, black dots). For CCMV-Au7B VLPs, after 12 min reduction time, the initial reaction rate constant was calculated to be $k_{CCMV-Au7B} = 2.1 \times 10^{-3} \pm 6.1 \times 10^{-5}$ min^{-1}. This rate constant is lower than the one found for bare Au NPs ($k_{Au} = 8.2 \times 10^{-2} \pm 2.5 \times 10^{-3}$ min^{-1}), presumably due to the diffusion barrier imposed by the protein shell (Figure 2g).[24] Surprisingly, the CCMV-Au7B film showed a higher catalytic activity compared to CCMV-Au7B VLPs with $k_{CCMV-Au7B\ film} = 4.3 \times 10^{-2} \pm 7.2 \times 10^{-4}$ min^{-1}. The relatively high catalytic activity of the film might be caused by a more acidic local environment compared to the bulk solution, resulting from the conversion of basic amine groups in the protein shells by crosslinking and the additional carboxylic acids from hydrolysis of the partially reacted TMC molecules. Such a local acidic environment can promote the hydrolysis of NaBH$_4$ and thus enhance the reduction reaction.[36–38] These results do clearly indicate that the catalytic activity of Au NPs can be maintained in the compartments within the films created by cross-linking the protein cages, which allows for further applications in, e.g., catalytic or sensor devices.[39–41]

2.4. Compartmentalized Thin Films with Horseradish Peroxidase Loaded

To further demonstrate the tunable functionality of protein cage-based compartmentalized films, HRP was introduced as a representative enzyme (**Figure 3**a). To encapsulate HRP into the CCMV based protein cage, HRP was first functionalized with negatively charged polystyrene sulfonate (PSS) and encapsulated in analogy with the procedure reported by Brasch et al.[42] To this end a polymer prepared by atom transfer radical polymerization (ATRP) from a disulfide based initiator (PSS-SS-PSS) was in situ reduced and coupled to HRP modified with a reactive maleimide moiety. HRP, HRP$_{PSS}$, and CCMV-HRP$_{PSS}$ were purified and studied by fast protein liquid chromatography (FPLC). HRP eluted at $V = 18$ mL (Figure S7, Supporting Information, top image). The elution volume of HRP$_{PSS}$ was the same, while the absorption at $\lambda = 260$ nm increased (Figure S7, Supporting Information, bottom image), in line with the conjugating of PSS. The excess of PSS eluted at $V = 13$ mL, presumably in aggregated form. The HRP$_{PSS}$ fraction with $V = 18$–19 mL was collected for encapsulation. From the HRP$_{PSS}$-coat protein mixture, three fractions were isolated: 1) $V = 9.5$ mL likely corresponding to aggregates or $T = 3$ VLPs; 2) $V = 12.5$ mL corresponding to $T = 1$ CCMV-HRP$_{PSS}$; 3) $V = 18.5$ mL corresponding to nonencapsulated HRP (Figure 3b). Fraction 2 was analyzed by TEM and dynamic light scattering (DLS), which both pointed to the formation of VLPs with $D = 18$ nm in line with a $T = 1$ structure (Figure 3c).[34] The presence of HRP was further confirmed by UV–vis spectroscopy, showing the characteristic absorption of the heme group at $\lambda = 403$ nm (Figure 3d) and by sodium dodecyl sulfate polyacrylamide gel electrophoresis (SDS-PAGE) (Figure S8, Supporting Information).

The encapsulation efficiency of enzyme per capsid was 92%. (see Section S1.3.2, Figure S9, Supporting Information).

A CCMV-HRP-based film was prepared as described for the other protein cage systems, yielding a material with an average thickness of 21.3 ± 3.5 nm measured by AFM (Figure 3e, f). This is close to the particle diameter $D = 18$ nm, suggesting a CCMV-HRP$_{PSS}$ monolayer. The HRP activity in the obtained thin film was studied by oxidation of 2,2′-azino-bis(3-ethylbenzothiazoline-6-sulphonic acid) (ABTS) (Figure 3g). All reactions were carried out in Tris-HCl buffer (10×10^{-3} M Tris,10×10^{-3} M NaCl, pH 7.5) and monitored by UV–vis, following the characteristic ABTS radical cation absorption at $\lambda = 420$ nm. 100 µL of a catalyst dispersion, with a concentration of 2×10^{-9} M HRP (total number of enzymes, 1.20×10^{11}) was used to determine the reaction rate as a function of substrate concentration (Figure 3g, left image). HRP, HRP$_{PSS,}$ and CCMV-HRP$_{PSS}$ all follow Michaelis-Menten kinetics with $V_{max} = (750 \pm 71) \times 10^{-9}$, $(515 \pm 49) \times 10^{-9}$, and $(330 \pm 30) \times 10^{-9}$ M s^{-1}, respectively. The reduction in rate is tentatively ascribed to hamper accessibility of the substrate to the enzyme's active site by the polymer and/or the protein cage. The oxidation product, i.e., the ABTS radical cation, is green, allowing direct visualization in the cuvette (Figure S10, Supporting Information). A thin film was attached on one side of the inner wall of the cuvette and after addition of a H$_2$O$_2$/ABTS mixed solution, a green color was generated on the surface of the film and which then diffused into bulk solution. The catalytic activity of the CCMV−HRP$_{PSS}$ thin film was quantitatively studied using a multiplate reader. The CCMV-HRP$_{PSS}$ film initially showed an increasing reactivity with increasing ABTS concentration (0–2.18×10^{-3} M), but the reaction rate decreases when the concentration exceeds 3.13×10^{-3} M, probably due to product inhibition.[43–45] The highest rate with $v = (196 \pm 29) \times 10^{-9}$ M s^{-1} was found at [ABTS] = 2.18×10^{-3} M (Figure 3g, right image). The corresponding turn-over numbers for HRP, HRP$_{PSS}$, CCMV-HRP$_{PSS}$, and the CCMV-HRP$_{PSS}$ thin film were calculated as $(6.2 \pm 0.4) \times 10^{-9}$, $(4.3 \pm 0.4) \times 10^{-9}$, $(2.7 \pm 0.2) \times 10^{-9}$, and $(2.2 \pm 0.3) \times 10^{-9}$ nM· (s·per enzyme)$^{-1}$ (Figure 3h). This analysis shows that the activities of the different HRP systems are within the same order of magnitude, where it should be noted that the concentration of enzyme in the film is expected to be lower. It is evident from the observed catalytic conversions that upon the incorporation of HRP in the protein cage based films, the transport of substrates and products between the bulk solution and the internal compartments of the films is still possible.

3. Conclusion

We have successfully constructed compartmentalized thin films by simple and straightforward interfacial cross-linking of viral protein cages. The thickness of the films can be controlled through the reaction conditions. The employment of the CCMV protein cage provides materials with defined compartments in the free-standing thin films, which not only helps to quantify and stabilize the cargo, but also equips the films with customized functionality. As a prove of concept, gold nanoparticles and HRP enzyme were effectively integrated into such thin films, respectively, which display catalytic activity as expected. Beyond what we have demonstrated here, we
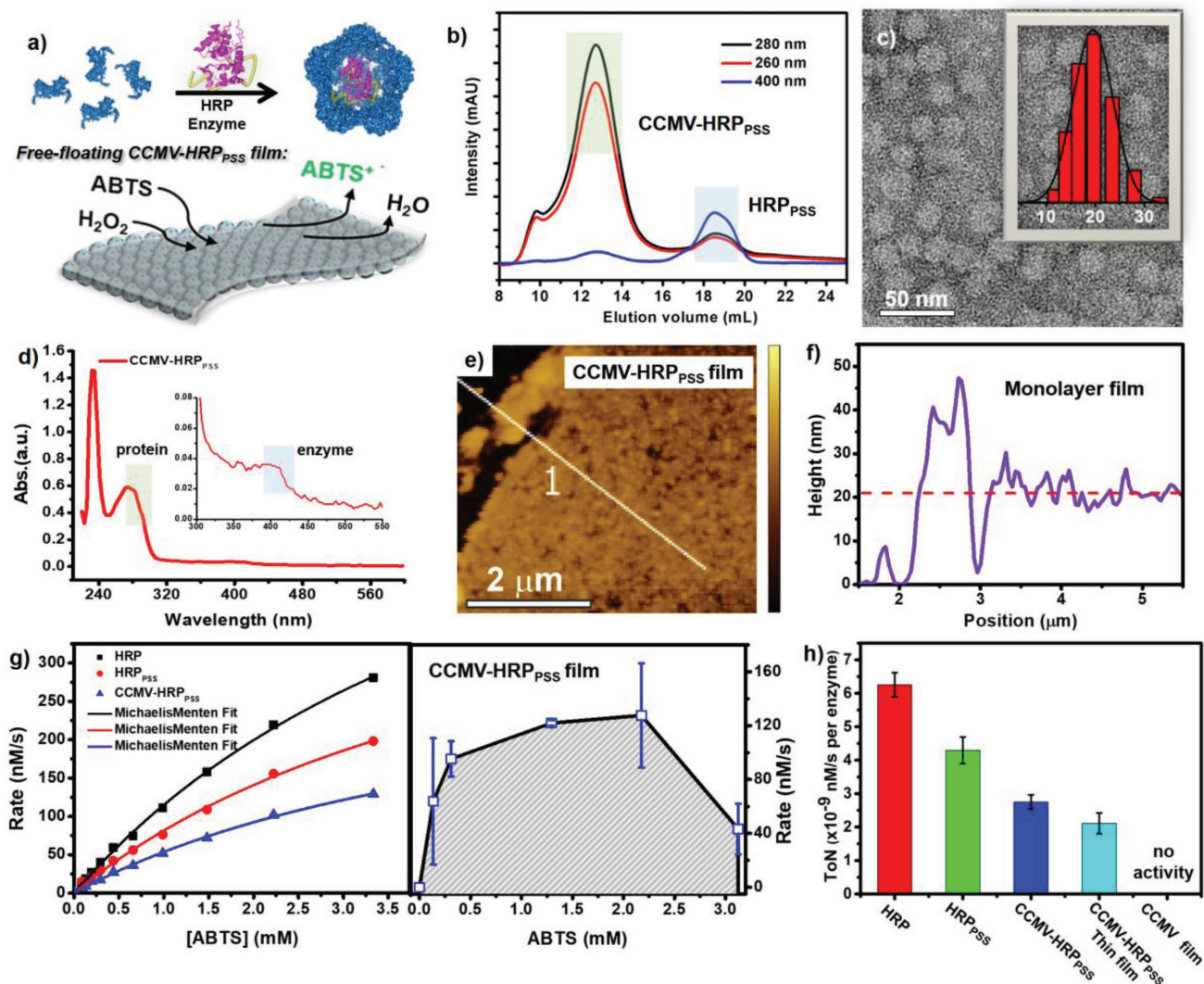
Figure 3. a) Schematic illustration of the fabrication of CCMV-HRPP$_{SS}$ free-standing thin film; b) FPLC size exclusion chromatograms for HRP$_{PSS}$ and CCMV-HRP$_{PSS}$; c) TEM image of CCMV-HRP$_{PSS}$, insert: the related DLS distribution; d) UV–vis spectra of CCMV-HRPP$_{SS}$; e,f) AFM analysis of CCMV-HRPpss monolayer free-standing thin film; g) Mechaelis-Menten plot for reaction rate of HRP, HRP$_{PSS}$ and CCMV-HRP$_{PSS}$ NPs (left), CCMV-HRP$_{PSS}$ film (right); h) Turn over numbers of free HRP, HRP$_{PSS}$, CCMV-HRP$_{PSS}$ and CCMV-HRPpss film.

believe this versatile strategy is also available for other (bio)-organic nanocontainers, a wide range of cargos and it is easily applied in devices (e.g., via conformal coating) potentially leading towards application in optical electronic devices, biosensors, wastewater treatment, and biomedical materials.

4. Experimental Section

Materials: Reagents and reactants that were purchased from Sigma Aldrich are used without further purification. Water used for buffer and reactions was of MilliQ quality (Millipore, $R = 18.2$ MΩ cm^{-1}). Quartz glass cuvettes were purchased from Hellma-analytics, Quartz SUPRASIL (QS), for UV–vis analysis. Tannic acid and citric acid stabilized gold nanoparticles were purchased from NanoComposix with mass concentration of 0.05 mg mL^{-1}, dispersed in MilliQ water. Amicon Ultra centrifuge filters with 10 kDa MWCO were purchased from Pall Corporation. Polyacrylonitrile ultrafiltration membrane (PAN) were purchased from SolSep, Netherlands.

Bis-p-(sufonatophenyl) Phenyl Phosphine (BSPP) Ligand Exchange: BSPP capped nanoparticles were prepared according to the previous report.[27] Briefly, BSPP (4 mg, 7.5 μmol) was dissolved in Milli-Q (1 mL), and then added to citric acid stabilized gold nanoparticle aqueous solution (10 mL, 0.05 mg mL^{-1}) under stirring. The stirring was continued overnight at room temperature (r.t). After then, citric acid was removed by washing with aqueous BSPP (1×10^{-3} M) three times using 10 kDa MWCO centrifuge filter, followed by washing with MQ two times to remove the excess of BSPP.

CCMV–Au Hybrid VLPs: In a typical experiment, a AuNP solution (400 μL, 0.5 mg mL^{-1}) was added to a solution of CCMV coat protein (100 μL, 15 mg mL^{-1}; pH 7.5; 50×10^{-3} M Tris, 500×10^{-3} M NaCl) and incubated for 5 min at r.t. The reaction mixture was subsequently incubated overnight at 4 °C. The resulting VLPs were purified using preparative fast protein liquid chromatography (FPLC). Tannic acid stabilized 7 nm gold nanoparticles encapsulated hybrid nanoparticles are represented by CCMV-Au7T, and BSPP stabilized 7 nm gold nanoparticles encapsulated hybrid nanoparticles are represented by CCMV-Au7B.

Disulfide-Containing Polystyrene Sulfonate (PSS-SS-PSS): Sodium 4-styrenesulfonate monomer (4.89 g, 21.3 mmol) and

bis[2-(2′-bromoisobutyryloxy)ethyl]disulfide initiator (106 mg, 0.23 mmol) were dissolved in water (21 mL) in a round-bottomed flask. The solution was then purged with nitrogen gas for 30 min. During this time, an excess of methanol was also purged with nitrogen gas. After 30 min, methanol (7 mL) was injected into the monomer/initiator solution using a nitrogen-purged syringe. The solution was then purged with nitrogen gas for additional 5 min. Cu(I)Br (68 mg, 0.47 mmol) and 2,2′-bipyridine ligand (148 mg, 0.95 mmol) were added together as solids, while maintaining a slow nitrogen purge. After 24 h, the catalyst was removed by flash column chromatography (eluent $MeOH/H_2O$ (1:1), 4 column volumes at least). After concentration, polymer was precipitated in cold THF and dried overnight at 60 °C.

HRP-PSS (HRP_{PSS}) Conjugation: 10.8 mg of PSS (20 kDa) containing a disulfide group and 4 mg DTT (PSS:DTT = 1:50, mol mol^{-1}) were dissolved in PBS buffer (10×10^{-3} M PB, 0.1 M NaCl). The solution was incubated for 2 h at r.t to the reduce disulfide bond. After 2 h of reaction, DTT was removed by washing with PBS buffer (at least 3 times) through Amicon Ultra centrifuge filters (2 kDa MWCO). In parallel, sulfo-EMCS modified HRP was prepared. 510 µg of HRP (1.26×10^{-8} mol) and 370 µg of sulfo-EMCS (9×10^{-7} mol) were dissolved in 0.5 mL of PBS buffers separately. The above two solutions were then mixed and incubated at r.t for 1 h on a roller bank. After that, the excess of sulfo EMCS was removed by using Zeba Spin Desalting Columns (7 kDa MWCO). Sulfo-EMCS modified HRP was then mixed with PSS-HS and incubated for 1–2 h at r.t on the roller bank. Purification of HRPPSS was carried out by fast protein liquid chromatography (FPLC) with elution buffer (25×10^{-3} M Tris, 25×10^{-3} M NaCl, 5×10^{-3} M KCl, 2.5×10^{-3} M $MgCl_2$, pH 7.5).

CCMV-HRP_{PSS} Hybrid VLPs: HRP_{PSS} and free coat protein (in 250×10^{-3} M Tris, 250×10^{-3} M NaCl, 50×10^{-3} M $MgCl_2$, pH 7.5) were mixed in a volume ratio of 5:1, the final molar ratio of HRPPSS to coat protein is 1:180. The mixture was then incubated for at least 3 h at 4 °C, afterwards, purification was carried out by FPLC with elution buffer (50×10^{-3} M Tris, 50×10^{-3} M NaCl, 10×10^{-3} M KCl, 5×10^{-3} M $MgCl_2$, pH7.5).

Compartmentalized Thin-Film Based on CCMV: Thin films were prepared by interfacial cross-linking.[3] The bottom aqueous phase contained 1.5 mg mL^{-1} of CCMV nanoparticles in 0.2 M phosphate buffer (PB, pH7.2) solution, and the top oil phase contained TMC solution in hexane. In the reactant concentration-dependent study, TMC concentration was varied from 0.125 to 1.1 wt%. In the time-dependent study, the reaction time was varied till 35 min. The formed thin films were transferred for further study.

CCMV–Au Hybrid VLPs Based Thin Film: 300 µL of CCMV–Au solution (concentration based on Au NPs, 0.05 mg mL^{-1} of Au NPs in 0.2 M PB buffer, pH 7.2) was added into a quartz cuvette. The same volume of 0.25 wt% of TMC hexane solution was added on the top and the reaction was continued for 15 min. Afterwards, the film was removed from the solution and rinsed with PB buffer once (be careful! The thin film may be removed together with the washing solution). Afterwards, the thin film was transferred for further analysis or left in the cuvette for further study.

CCMV-HRP_{PSS} Hybrid VLPs Based Thin Film: 100 µL of CCMV-HRP_{PSS} solution (in 0.2 M PB buffer, pH 7.2) with various concentrations was added into a quartz cuvette or in a Corning flat bottom 96-well UV transparent plate. 0.25 wt% of TMC hexane solution was added on the top and the reaction was kept for 15 min. Both solutions were removed and the thin film was washed with PB buffer once (be careful! Thin film may be removed together with the washing solution) for further study.

Reduction Reaction Catalyzed by AuNPs, CCMV-Au VLPs, and CCMV-Au Thin Film: 1.2 mL of MilliQ was added into a quartz cuvette with a thin film attached on one inner side, UV–vis recording was started right after adding of 300 µL of $NaBH_4$ and 4NP mixture. Total number of Au NPs in monolayer of thin film was calculated (see Section S3.2.2, Supporting Information). In a control experiment, 1.2 mL of Au NPs/CCMV-Au VLPs (contained the same number of Au NPs as in the thin film) was mixed with 300 µL of $NaBH_4$ and 4NP mixture, reactions were recorded by UV–vis as well.

Kinetic Study of Reactions Catalyzed by HRP, HRP_{PSS}, CCMV-HRP_{PSS}, and CCMV-HRP_{PSS} Thin Films by Multiplate Reader: All reactions catalyzed by HRP, HRP_{PSS}, CCMV-HRP_{PSS} free VLPs, and the corresponding thin films were performed in Tris–HCl buffer, which is 25×10^{-3} M Tris, 25×10^{-3} M NaCl, 5×10^{-3} M KCl, 2.5×10^{-3} M $MgCl_2$, pH 7.5.

HRP, HRP_{PSS}, CCMV-HRP_{PSS} VLPs: 50 µL solutions with 4×10^{-9} M HRP (or HRP_{PSS}, CCMV-HRP_{PSS}) and 10×10^{-3} M H_2O_2 were added into 96 well plates, UV–vis monitoring on a TECAN I-control multiplate reader was started immediately after adding 50 µL of ABTS substrates with various concentrations.

CCMV-HRP_{PSS} Thin Films: 100 µL of 5×10^{-3} M H_2O_2 was added into the well which contained the CCMV-HRP_{PSS} thin films. Kinetic assay was performed by adding 18×10^{-3} M of ABTS with various volumes to obtain various final concentration of substrates. The concentration changes of CCMV-HR_{PPSS} and H_2O_2 were negligible since only small volume (<10 µL) of ABTS solution was added.

Characterization Methods—Fast Protein Liquid Chromatography: Samples were purified and collected on an Aktapurifier (Box-900) equipped with a Superose 6 10/100 GL column (GE Healthcare) in a 0.5 mL min^{-1} flow rate and a fraction collector (Frac-950).

(S)TEM Analysis: TEM samples were prepared by drop casting. In general, 5 µL of sample solution was dropped onto formvar carbon coated copper grid. After 5 min incubation, the remaining liquid was removed by tipping the grid onto a low lint paper (Kimtech science precision wipes). The sample was stained using 5 µL of a 1 wt% uranyl acetate solution for 30 s to provide optimal contrast. Sample was imaged using a Philips CM300ST-FEG TEM or a Zeiss Merlin (S)TEM. The resulting images were analyzed using ImageJ software to determine the size of particles and gold cores.

Dynamic Light Scattering: Each sample was measured using an Anaspec Nanotrac Wave dynamic light scattering instrument for five times and the average was report. Protein refractive index was set to be 1.54.

Atomic Force Microscopy: Thin films were carefully transferred on top of silicon wafer and dried under clean environment before analysis. AFM measurements were performed using a Multimode AFM (Bruker Nano Surfaces, Santa Barbara, CA, USA) with a NanoScope V controller under tapping mode.

Calculation of Turn over Number—Total Number of HRP in the CCMV-HRP_{PSS} Thin Film: Monolayer of thin films was prepared inside wells with an identical diameter of 0.57 cm. Therefore, each thin film contained ≈1.01E+11 of VLPs (18 nm). Given that the HRP loading efficiency was 92%, each thin film contained ≈9.20E+10 of HRP. The numbers of enzymes in 100 µL of 2×10^{-9} M HRP, HRP_{PSS}, and CCMV-HRP_{PSS} VLPs were all at 1.20E+11.

Turn over number of HRP_{PSS}, CCMV-$HRP_{PSS,}$ and CCMV-HRP_{PSS} thin film = $V_{max}/$(number of enzyme).

Supporting Information

Supporting Information is available from the Wiley Online Library or from the author.

Acknowledgements

Conflict of Interest

The authors declare no conflict of interest.

[1] M. F. Jimenez-Solomon, Q. Song, K. E. Jelfs, M. Munoz-Ibanez, A. G. Livingston, *Nat. Mater.* **2016**, *15*, 760.

[2] J. Hong, S. Lee, J. Seo, S. Pyo, J. Kim, T. Lee, *Mater. Interfaces* **2015**, *7*, 3554.

[3] M. J. T. Raaijmakers, T. Schmidt, M. Barth, M. Tutus, N. E. Benes, M. Wessling, *Angew. Chem., Int. Ed.* **2015**, *54*, 5910.

[4] Y. Lin, H. Skaff, A. Böker, A. D. Dinsmore, T. Emrick, T. P. Russell, *J. Am. Chem. Soc.* **2003**, *125*, 12690.

[5] J. Troyano, L. Hu, T. D. Keiper, P. Xiong, D. T. Hallinan, *J. Mater. Chem. C* **2016**, *4*, 8545.

[6] G. Yang, L. Hu, T. D. Keiper, P. Xiong, D. T. Hallinan, *Langmuir* **2016**, *32*, 4022.

[7] S. Vozar, Y.-C. Poh, T. Serbowicz, M. Bachner, P. Podsiadlo, M. Qin, E. Verploegen, N. Kotov, A. J. Hart, *Rev. Sci. Instrum.* **2009**, *80*, 023903.

[8] T. S. Shim, Z. G. Estephan, Z. Qian, J. H. Prossor, S. Lee, D. M. Chenowethm, D. Lee, S.-J. Park, J. C. Crocker, *Nat. Nanotechnol.* **2017**, *12*, 41.

[9] J. Zhang, B. Yuan, Z. Wang, T. Chen, *Colloid Polym. Sci.* **2014**, *292*, 1235.

[10] Z. G. Estephan, Z. Qian, D. Lee, J. C. Crocker, S.-J. Park, *Nano Lett.* **2013**, *13*, 4449.

[11] T. Andryszewski, M. Iwan, M. Hołdyński, M. Fiałkowski, *Chem. Mater.* **2016**, *28*, 5304.

[12] P. Fromherz, *Nature* **1971**, *231*, 267.

[13] H. Yoshimura, T. Scheybani, W. Baumeister, K. Nagayama, *Langmuir* **1994**, *10*, 3290.

[14] H. Yoshimura, *Adv. Biophys.* **1997**, *34*, 93.

[15] J. T. Russell, *Angew. Chem., Int. Ed.* **2005**, *44*, 2420.

[16] G. Kaur, Y. Lin, A. Böker, L. Su, P. Carl, H. Zettl, J. He, K. Sill, R. Tangirala, T. Emrick, K. Littrell, P. Thiyagarajan, D. Cookson, A. Fery, Q. Wang, T. P. Russell, *Langmuir* **2009**, *25*, 5168.

[17] J. He, Z. Niu, R. Tangirala, J.-Y. Wang, X. Wei, G. Kaur, Q. Wang, G. Jutz, A. Böker, B. Lee, S. V. Pingali, P. Thiyagarajan, T. Emrick, T. P. Russell, *Langmuir* **2009**, *25*, 4979.

[18] P. van Rijn, H. Park, K. Özlem Nazli, N. C. Mougin, A. Böker, *Langmuir* **2013**, *29*, 276.

[19] P. van Rijn, M. Tutus, C. Kathrein, N. C. Mougin, H. Park, C. Hein, M. P. Schürings, A. Böker, *Adv. Funct. Mater.* **2014**, *24*, 6762.

[20] H. Yoshimura, E. Edwards, M. Uchida, K. McCoy, R. Roychoudhury, B. Schwarz, D. Patterson, T. Douglas, *J. Phys. Chem. B* **2016**, *120*, 5938.

[21] C. M. Soto, B. R. Ratna, *Curr. Opin. Biotechnol.* **2010**, *21*, 426.

[22] T. Ueno, M. Suzuki, T. Goto, T. Matsumoto, K. Nagayama, Y. Watanabe, *Angew. Chem., Int. Ed.* **2004**, *43*, 2527.

[23] P. C. Jordan, D. P. Patterson, K. N. Saboda, E. J. Edwards, H. M. Miettinen, G. Basu, M. C. Thielges, T. Douglas, *Nat. Chem.* **2016**, *8*, 179.

[24] A. Liu, C. H. H. Traulsen, J. J. L. M. Cornelissen, *ACS Catal.* **2016**, *6*, 3084.

[25] M. Comellas-Aragones, H. Engelkamp, V. I. Claessen, N. A. J. M. Sommerdijk, A. E. Rowan, P. C. M. Christianen, J. C. Maan, B. J. M. Verduin, J. J. L. M. Cornelissen, R. J. M. Nolte, *Nat. Nanotechnol.* **2007**, *2*, 635.

[26] A. M. Wen, N. F. Steinmetz, *Chem. Soc. Rev.* **2016**, *45*, 4074.

[27] A. Liu, M. Verwegen, M. V. de Ruiter, S. J. Maassen, C. H. H. Traulsen, J. J. L. M. Cornelissen, *J. Phys. Chem. B* **2016**, *120*, 6352.

[28] M. Brasch, A. de la Escosura, Y. Ma, C. Uetrecht, A. J. R. Heck, T. Torres, J. J. L. M. Cornelissen, *J. Am. Chem. Soc.* **2011**, *133*, 6878.

[29] F. Setaro, M. Brasch, U. Hahn, M. S. T. Koay, J. J. L. M. Cornelissen, A. de la Escosura, T. Torres, *Nano Lett.* **2015**, *15*, 1245.

[30] X. Huang, L. M. Bronstein, J. Retrum, C. Dufort, I. Tsvetkova, S. Aniagyei, B. Stein, G. Stucky, B. McKenna, N. Remmes, D. Baxter, C. C. Kao, B. Dragnea, *Nano Lett.* **2007**, *7*, 2407.

[31] C. A. Hommersom, B. Matt, A. van der Ham, J. J. L. M. Cornelissen, N. Katsonis, *Org. Biomol. Chem.* **2014**, *12*, 4065.

[32] B. J. M. Verduin, *J. Gen. Virol.* **1978**, *39*, 131.

[33] X. Huang, M. A. El-Sayed, *J. Adv. Res.* **2010**, *1*, 13.

[34] K. L. Wustholz, A.-I. Henry, J. M. McMahon, R. G. Freeman, N. Valley, M. E. Piotti, M. J. Natan, G. C. Schatz, R. P. V. Duyne, *J. Am. Chem. Soc.* **2010**, *132*, 10903.

[35] S. S. Masango, R. A. Hackler, N. Large, A.-I. Henry, M. O. McAnally, G. C. Schatz, P. C. Stair, R. P. Van Duyne, *Nano Lett.* **2016**, *16*, 4251.

[36] M. Li, G. Chen, *Nanoscale* **2013**, *5*, 11919.

[37] S. Choi, Y. Jeong, J. Yu, *Catal. Commun.* **2016**, *84*, 80.

[38] F.-H. Lin, R.-A. Doong, *Appl. Catal., A* **2014**, *486*, 32.

[39] K. Saha, S. S. Agasti, C. Kim, X. Li, V. M. Rotello, *Chem. Rev.* **2012**, *112*, 2739.

[40] R. Sharma, M. A. Ali, N. R. Selvi, V. N. Singh, R. K. Sinha, V. V. Agrawal, *J. Phys. Chem. C* **2014**, *118*, 6261.

[41] S. R. Ahmed, J. Kim, V. T. Tran, T. Suzuki, S. Neethirajan, J. Lee, E. Park, *Sci. Rep.* **2017**, *7*, 44495.

[42] M. Brasch, R. M. Putri, M. V. de Ruiter, D. Luque, M. S. T. Koay, J. R. Castón, J. J. L. M. Cornelissen, *J. Am. Chem. Soc.* **2017**, *139*, 1512.

[43] S. V. Rao, K. W. Anderson, L. G. Bachas, *Biotechnol. Bioeng.* **1999**, *65*, 389.

[44] B. Limoges, J.-M. Savéant, D. Yazidi, *J. Am. Chem. Soc.* **2003**, *125*, 9192.

[45] R. E. Childs, W. G. Bardsley, *Biochem. J.* **1975**, *145*, 93.